J. W. Storer, D. J. Giesen, G. D. Hawkins, G. C. Lynch, C. J. Cramer, D. G. Truhlar, and D. A. Liotard, in *Structure, Energetics, and Reactivity in Aqueous Solution: Characterization of Chemical and Biological Systems*, edited by C. J. Cramer and D. G. Truhlar (American Chemical Society Symposium Series 568, Washington, DC, 1994), pp. 24-49.

Solvation Modeling in Aqueous and Nonaqueous Solvents

New Techniques and a Reexamination of the Claisen Rearrangement

Joey W. Storer[1], David J. Giesen[1], Gregory D. Hawkins[1], Gillian C. Lynch[1], Cristopher J. Cramer[1], Donald G. Truhlar[1], and Daniel A. Liotard[2]

[1]Department of Chemistry and Supercomputer Institute, University of Minnesota, 207 Pleasant Street, S.E., Minneapolis, MN 55455–0431
[2]Laboratoire de Physico-Chimie Theorique, Université de Bordeaux 1, 351 Cours de la Liberation, 33405 Talence Cedex, France

This chapter presents an overview of recent improvements and extensions of the quantum mechanical generalized-Born-plus-surface-tensions (GB/ST) approach to calculating free energies of solvation, followed by a new treatment of solvation effects on the Claisen rearrangement. The general improvements include more efficient algorithms in the AMSOL computer code and the use of class IV charge models. These improvements are used with specific reaction parameters to calculate the solvation effect on the Claisen rearrangement both in alkane solvent and in water, and the results are compared to other recent work on this reaction.

1. Introduction

The kinds of reaction pathways that one typically encounters in aqueous solution often differ qualitatively from those in the gas phase or in nonpolar solvents, even when water does not play a structural or catalytic role in the chemical reaction. Much of the controlling influence of the solvent in aqueous chemistry can be understood in terms of the thermodynamic solvation parameters of reactants, products, and transition states. Thus, as is so often the case in chemistry, a reasonable starting point for a quantitative understanding of chemical processes occurring in aqueous solution is the thermochemistry *(1,2)*. Chemical equilibria are controlled by free energies, and rates—according to transition state theory *(3)*—are controlled by free energies of activation, so the free energies of hydration are the central quantities in the thermochemistry. This chapter is primarily concerned with the free energy of aqueous solvation, also called the free energy of hydration. We also consider the free energy of solvation in a nonpolar condensed medium, in particular hexadecane.

0097–6156/94/0568–0024$09.08/0

Our discussion is focused on a class of quantum mechanical–continuum dielectric models, called the SM*x* models *(4-10)*. The original versions were SM1 *(4)*, SM1A *(4)*, SM2 *(5)*, and SM3 *(6)*, a newer version is SM2.1 *(8)*, and a version under development is SM4A *(9)*. These versions are all for water solvent. Parameterized versions for hexadecane solvent, called SM4C *(10)* and SM4A *(9)* (the latter having the same coulomb radii as the water SM4A model, and hence sharing the same name), are also under development. These models are concerned with transfer of a solute from the gas-phase into dilute solution. They are based on a quantum mechanical treatment of the internal electronic structure of a solute combined with a treatment of the solvent modeled as a nonhomogeneous continuum. The nonhomogeneity is very simple, consisting of an environment-specific first hydration shell superimposed on a homogeneous bulk dielectric medium. The interaction of the solute with the dielectric continuum is treated by classical electrostatics using partial charges on solute atoms, calculated either by Mulliken analyses *(11-13)* of neglect-of-diatomic-overlap *(14-17)* (NDDO) electronic wave functions or by new class IV charge models *(18)* based on semiempirical mappings of quantum mechanically derived partial charges.

The general framework of the SM*x* models is described extensively elsewhere, especially in overviewing *(7,19,20)* the SM2 and SM3 models, so this basis is reviewed only briefly here. This is done in Section 2, which also briefly reviews the difference of the aqueous models from the models (SM4C *(10)*, SM4A *(9)*) developed for hexadecane. Section 3 reviews recent algorithmic improvements *(8)* in the implementation of these models in the AMSOL code *(21)*. Section 4 reviews a new charge model *(18)*, which is used in the SM*x* models for $x = 4$.

Section 5 presents our first example of a new approach to solvation modeling, namely the use of parameters for a specific reaction or a specific range of solutes. This is called specific-reaction or specific-range parameterization (SRP) to distinguish it from using general parameterizations such as SM2.1 or SM4A, which have compromise parameters designed to model a broad range of solutes with a single parameter set. By targeting a specific range of solutes or reactions, the new approach allows faster parameterization and more accurate semiempirical predictions for the targeted systems. Section 6 presents an application of the SRP parameters of Section 5 to the Claisen reaction and compares the results to other recent work.

2. The SM2 and SM3 Models

In the SM2 and SM3 solvation models, we calculate the standard-state solvation free energy ΔG^o_S as a sum of two terms

$$\Delta G^o_S(aq) = \Delta G_{ENP}(aq) + G^o_{CDS}(aq) \quad (1)$$

where

$$\Delta G_{ENP}(aq) = \Delta E_{EN}(aq) + G_P(aq). \quad (2)$$

$\Delta E_{EN}(aq)$ is the change in the internal electronic kinetic and electronic and nuclear coulombic energy of the solute upon relaxation in solution, which is driven by the favorable electric polarization interaction with the solvent. $G_P(aq)$ is the electric

polarization free energy, including both this favorable solute-solvent interaction and the unfavorable change in solvent molecule-solvent molecule interactions. Finally, G^o_{CDS} is the cavitation-dispersion-solvent-structural free energy.

In $\Delta G_{ENP}(aq)$, the solvent is treated as a continuum dielectric with bulk properties, and ΔG_{ENP} itself is the net favorable resultant free energy change due to bulk volume electrostatic effects. The solute internal, solvent internal, and solute-solvent effects are treated self-consistently by including the thermodynamic electrostatic effect as an operator in a self-consistent-field (SCF) semiempirical molecular orbital (MO) calculation on the solute, and this MO calculation is carried out by either of two popular parameterized models, namely Austin Model 1 (AM1) *(16)* or Parameterized Model 3 (PM3) *(17)*.

The second term in eq. 1, G^o_{CDS}, accounts for deviations from the first term due to the fact that the molecules in the first hydration shell of the solvent do not behave in the same way as the bulk dielectric. Thus, it includes the free energy of cavity formation, the short-range solute-solvent dispersion forces, and solvent-structure changing effects such as hydrogen bonding, the tightening of the first hydration shell around hydrophobic solutes, and the different degree of solvent polarization in the first hydration shell as compared to the bulk.

We approximate $G_P(aq)$ by a version of the generalized *(22-25)* Born *(26)* equation. This is a generalization of Born's treatment of a monatomic ion immersed in a dielectric medium. The generalization requires a form for two-center interactions in the dielectric medium and for treating the screening of some parts of the solute from the dielectric by other parts of the solute. Our treatment of these aspects of the generalization is based on the work of Still et al. *(27)*. The generalized Born equation is given by

$$G_P(aq) = -\frac{1}{2}\left(1-\frac{1}{\varepsilon}\right)\sum_{i,i'} q_i q_{i'} \gamma_{ii'}, \tag{3}$$

where ε is the solvent dielectric constant, q_i is the net atomic partial charge on atom i of the solute, and $\gamma_{ii'}$ is a one-center ($i = i'$) or two-center ($i \neq i'$) coulomb integral. In the SM*x* models, these integrals are given by

$$\gamma_{ii'} = \{r_{ii'}^2 + \alpha_i \alpha_{i'} C_{ii'}(r_{ii'})\}^{-1/2}, \tag{4}$$

where α_i is the radius of the Born sphere associated with atom i, $r_{ii'}$ is the interatomic distance between atoms i and i', $C_{ii'}(r_{ii'})$ is given by

$$C_{ii'}(r_{ii'}) = C_{ii'}^{(0)}(r_{ii'}) + C_{ii'}^{(1)}(r_{ii'}), \tag{5}$$

where

$$C_{ii'}^{(0)} = \exp(-r_{ii'}^2/d^{(0)}\alpha_i\alpha_{i'}), \tag{6}$$

$d^{(0)}$ is an empirically optimized *(7)* constant equal to 4, and $C_{ii'}^{(1)}$ is given by

$$C_{ii'}^{(1)} = \begin{cases} d_{ii'}^{(1)} \exp\left(-d_{ii'}^{(2)} \Big/ \left\{1-\left[r_{ii'}-r_{ii'}^{(1)}\Big/r_{ii'}^{(2)}\right]^2\right\}\right), & \left|r_{ii'}-r_{ii'}^{(2)}\right| < r_{ii'}^{(2)} \\ 0, & \text{otherwise.} \end{cases} \tag{7}$$

The constant $d_{ii'}^{(1)}$ is a new semiempirical element first introduced in SM1 *(4)* and is nonzero only for O–O and N–H interactions.

For the monatomic case, there is only a one-center term ($i = i' = 1$), and α_i is set equal to a semiempirically determined intrinsic Born radius, ρ_i, where

$$\rho_i = \rho_i^{(0)} + \rho_i^{(1)}\left[-\frac{1}{\pi}\arctan\frac{q_i + q_i^{(0)}}{q_i^{(1)}} + \frac{1}{2}\right] \tag{8}$$

and where $q_i^{(1)}$ has been fixed at 0.1. Notice that the intrinsic Born radius depends on the atomic charge q_i, which is an integer for monatomic solutes. However, we also use eq. 8 as a starting point for polyatomic solutes, in which case q_i is not an integer. In the multicenter case, α_i is determined numerically, following the dielectric screening model introduced by Still et al. *(27)*. In this procedure α_i is chosen so that the G_P derived as in a monatomic case is equal to the G_P obtained by integrating about the atom the difference in the electronic free energy density fields of the charge distribution isolated in a vacuum and immersed in the dielectric solvent. Thus we calculate

$$\alpha_i^{-1} = \int_{\rho_i}^{\infty} \frac{dr}{r^2} \frac{A(r,\{\rho_i\})}{4\pi r^2} \tag{9}$$

where $A(r,\{\rho_{i'}\})$ is the numerically determined exposed surface area of a sphere of radius r centered at atom i, i.e., that area *not* included in any spheres centered around other atoms when those spheres have radii given by the set $\{\rho_{i'}\}$. (A sphere with such a radius is called a Born sphere in Section 3.) This area times dr is the part of the volume of the shell from r to r + dr around atom i that is *in* the solvent.

The E, N, and P terms are obtained from the density matrix **P** of the aqueous-phase SCF calculation as

$$G_{ENP}(aq) = \frac{1}{2}\sum_{\mu\nu} P_{\mu\nu}\left(H_{\mu\nu} + F_{\mu\nu}\right) + \frac{1}{2}\sum_{i,i'\neq i} \frac{Z_i Z_{i'}}{r_{ii'}} \tag{10}$$

where **H** and **F** are respectively the one-electron and Fock matrices, μ and ν run over valence atomic orbitals, and Z_i is the valence nuclear charge of atom i (equal to the nuclear change minus the number of core electrons). The Fock matrix is given by

$$F_{\mu\nu} = F_{\mu\nu}^{(0)} + \delta_{\mu\nu}\left(1-\frac{1}{\varepsilon}\right)\sum_{i',\mu'\in i'}\left(Z_{i'} - P_{\mu'\mu'}\right)\gamma_{ii'}, \quad \mu \in i \tag{11}$$

where $\mathbf{F}^{(0)}$ is the gas-phase Fock matrix, and $\delta_{\mu\nu}$ is a Kronecker delta. $\mathbf{F}^{(0)}$ and $\mathbf{H}$ are the same as for gas-phase calculations *(14-17)*. The density matrix is determined self-consistently in the presence of solvent. Then

$$\Delta G_{ENP}(aq) = G_{ENP}(aq) - E_{EN}(g) \quad (12)$$

The remaining contribution to the free energy of solvation beyond $\Delta G_{ENP}(aq)$ for *all* SM*x* models is calculated from

$$G^{o}_{CDS}(aq) = \sum_{\lambda=1}^{\Lambda} \sum_{i'} \left\{ \sigma^{(0)}_{i'}(\lambda) + \sigma^{(1)}_{i'}(\lambda) \left[F_{i'}\left(b^{(i')}\right) \right] \right\} A_{i'}\left(\beta_{i'}(\lambda), R_S(\lambda), \{\beta_i\}\right) \quad (13)$$

where $\sigma^{(0)}_{i'}$ and $\sigma^{(1)}_{i'}$ are atomic surface tension parameters, λ is defined below, $\Lambda = 1$ for water and $\Lambda = 2$ for hexadecane, $F_{i'}$ is a function of the bond orders $b^{(i')}$ to atom i′, and $A_{i'}(\beta_{i'}(\lambda), R_S(\lambda), \{\beta_i\})$ is the solvent-accessible surface area for atom i′. The latter is defined as the exposed surface area of atom i′, which equals the exposed surface area of the atom-centered sphere with radius

$$\beta_{i'}(\lambda) = R_{i'} + R_S(\lambda) \quad (14)$$

where $R_{i'}$ is the van der Waals radius of atom i′, and $R_S(\lambda)$ is a solvent radius, taken for water as 1.4 Å. Exposed area is defined in this step as area that is *not* contained in any of the other atomic spheres when they also have radii given by eq. 14; this is why $A_{i'}$ depends on the full set of $\{\beta_i\}$. Notice that $A_{i'}$ represents the area of a surface through the first solvation shell around atom i′, and thus, for a continuum solvent, it is proportional to the average number of solvent molecules in the first hydration shell *(28-30)*. In this model then, dispersion, solute-solvent hydrogen bonding, and disruption of solvent-solvent hydrogen bonding, as in the hydrophobic effect, are all assumed proportional to the number of waters that fit in the first hydration shell. This was the original motivation for making the nonhomogeneous part of the contribution to the first-hydration-shell free energy proportional to solvent-accessible surface area.

The bond orders are defined as elements of the covalent bond index matrix *(31)* as follows:

$$\left(b^{(i')}\right)_i = B_{ii'}, \quad (15)$$

Note that the precise form of the function $F_{i'}$ in eq. 13 depends on which solvation model is under consideration. In the SM4-SRP model presented in section 5, all $\sigma^{(1)}_i$ are defined to be zero, so that no specification of $F_{i'}$ is required. This is a simplification relative to SM2, SM2.1, and SM3.

The essential physics behind the assumption that eq. 13 can represent the hydrophobic effect is consistent with a recent simulation study *(32)* of the hydration entropy of inert gases, which are often taken as atomic examples of hydrophobic solutes. This study showed that the solute-water orientational correlations are essentially confined to the first hydration shell and, within about 15%, are proportional to the number of water molecules in the first hydration shell. This is very

encouraging although, of course, a more complete understanding of the first hydration shell must also take into account hydration enthalpies and the changes that occur for polar solutes. In a recent paper, Alary *et al. (33)* studied the hydration structure around a protein complex by molecular dynamics including 9154 explicit H_2O molecules. They found that the arrangement of first-shell water molecules strongly depends on the local nature of the protein surface and that the perturbation of the water structure by the protein essentially does not extend beyond one water layer. They concluded that the hydration structure in the immediate vicinity of any residue might be derived from data on this residue as a solute. All these conclusions are consistent with the present semiempirical approach in which the local surface tension, accounting for deviations from bulk solvent behavior in the first hydration shell, depends on the local character of the solute surface and is parameterized on the basis of small solutes.

For water, we use only one solvent radius, i.e., $\Lambda = 1$. In modeling solvation energies in hexadecane, on the other hand, we have used $\Lambda = 2$, with $R_S(1)$ representing the short range of the dispersion forces and $R_S(2)$ the long-range structural distortion of the solvent by the solute. This is a critical distinction between water and hexadecane. The water molecule, being small, is close enough to the solute for all its atoms to interact directly, whereas in a larger solute, dispersion affects only the closest subunits to the solute. Where $\Lambda = 2$, we may denote the solvent-accessible surface area calculated with $\lambda = 1$ as the area of the "dispersion shell" and solvent-accessible surface area calculated with $\lambda = 2$ as the area of the "structural solvation shell." For water both shells are taken as the traditional first solvation shell.

The parameters in the SM*x* models are adjusted to reproduce experimental data *(34-37)* for free energies of solvation. In parameterizing SM1, SM1a, SM2, and SM3, a specific approximately converged quadrature scheme was used for eq. 9, and the parameters made up for systematic deviations of these quadratures from converged ones. As discussed further below, the SM2.1 and SM4-type schemes are parameterized using well-converged quadratures.

3. Algorithms

A critical computational step that occurs repeatedly in the SM*x* solvation models, as just reviewed, is the calculation of the exposed surface area of an atom-centered sphere in the presence of several other spheres, centered at the other atoms of the solute. This step occurs in two contexts. First it occurs in the calculation of the electrostatic energy, where the singled-out sphere is either the Born sphere of one of the atoms or one of the enlarged spheres that occur as quadrature nodes in eq. 9, and the other spheres are the Born spheres of the other atoms. Second it occurs in the calculation of solvent-accessible surface areas of eq. 13 where the spheres are all van der Waals spheres augmented by the half-width, $R_S(\lambda)$, of the dispersion shell or structural solvation shell. In order to perform the calculations efficiently, we need an efficient algorithm to calculate these exposed surface areas and an efficient quadrature scheme for eq. 9. An efficient scheme for the latter will minimize the number of exposed surface areas to be calculated. Another way to minimize this number is by

employing efficient SCF convergers since the dielectric screening calculation is embedded in the SCF process.

We next summarize some recent improvements we have made that speed up the exposed-surface-area calculation and that minimize the number of such calculations required.

Exposed Surface Area Calculations. The AMSOL code allows a choice of 3 algorithms: DOTS, GEPOL, and ASA.

DOTS. The DOTS algorithm is discussed elsewhere *(7)*. It has been greatly speeded up since the first released version of AMSOL.

GEPOL. The GEPOL algorithm has also been discussed in detail elsewhere *(38,39)*.

ASA. The ASA algorithm *(8)* is based on an analytic calculation of each exposed surface area A_i. It has seven steps for a given sphere i:

(1) Using triangular inequalities on interatomic distances and sphere radii, we set up a list $L^{(1)}$ of spheres that intersect sphere i. If sphere i is completely embedded in another sphere or not intersected by any other sphere, A_i is either 0 or 4π times the radius squared, and steps 2-7 are not needed.

(2) We note that each sphere j that intersects i defines a spherical cap $SC_j^{(i)}$, which is the portion of the surface of i that is contained in j. For each sphere j that intersects sphere i, we calculate the cosine of the angle between the unit vector from the center I of i to the center J of j and a vector from I to any point on the circle of intersection of i and j.

(3) We define a connectivity matrix $\mathbf{C}^{(i)}$ whose element $C_{jk}^{(i)}$ is true if $SC_j^{(i)}$ intersects $SC_k^{(i)}$ and is otherwise false. Any spherical cap embedded entirely in another (larger) one or buried by two spherical caps is deleted from consideration at this stage.

(4) We calculate the buried surface area from isolated spherical caps and then delete them from $L_i^{(1)}$, making a new shorter list $L_i^{(2)}$.

(5) For each pair j, k of spheres in $L_i^{(2)}$ that intersect on the surface of i, we calculate unit vectors from I to the intersection points. We make a list of all such points that are not interior to any spherical cap $SC_l^{(i)}$ where $l \neq j, k$. These are called free junction points. Spherical caps that are buried by more than two other spherical caps are detected at this stage and deleted from $L_i^{(2)}$, making a shorter list $L_i^{(3)}$. Also at this stage we check for junction points that are nearly shared by the circular intersections with i of more than two spheres. If these are detected, the radius of sphere i is increased by a factor of 1×10^{-11} to avoid roundoff instabilities in a later step. In this step, special attention was paid to avoiding unnecessary calculations of trigonometric functions and to re-using information from previous steps where possible to save work.

(6) For each spherical cap in $L_i^{(3)}$, we select a free junction point from its circular boundary as a starting point. The angles from the starting point to the center of the circular intersection to each of the other free junction points are then calculated and sorted by magnitude. There is an odd number of such angles. The smallest such angle is either the vertex of a spherical polygon or the vertex of a spherical cap slice. If the smallest angle is due to a spherical cap slice, then the sum of the odd angles

minus the sum of the even angles can be used to determine the contribution to A_i from spherical cap slices. Otherwise, 2π minus this quantity is used.

(7) Using $\mathbf{C}^{(i)}$, we then count the number of spherical polygons, calculate the interior angles of each junction point vertex and add these to the sum of the interior angles of the intersection-centered vertices for the spherical polygons, the sum of the unused quantities in step 6. With this information, the contribution to A_i from spherical polygons can be calculated. Finally, by subtracting the surface area embedded in spherical caps, spherical cap sections, and spherical polygons, we obtain the exposed surface area of sphere i in a set of spheres.

Radial Quadratures for Dielectric Screening. The new algorithm for calculating the integral on the right side of eq. 9 begins by identifying a radius R for a sphere centered at I (the nucleus of atom i) such that a sphere of this radius would engulf all the Born spheres of the other atoms. Then we write

$$\frac{1}{\alpha_i} = \int_{\rho_i}^{R} dr \frac{a(r)}{r^2} + \frac{1}{R} \tag{16}$$

where

$$a(r) = \frac{A(r,\{\rho_k\})}{4\pi r^2}. \tag{17}$$

Next we define a sequence of quadrature segments $[b_{m-1}, b_m]$ by

$$b_m = \begin{cases} \rho_i, & m = 0 \\ b_{m-1} + T_1(1+F)^{m-1}, & m = 1,2,3,\ldots,M \end{cases} \tag{18}$$

where T_1 is determined by a two-step process. Starting with an input value of T_1 we calculate the minimum value of M such that $b_M \geq R$. Then for this M, we set

$$b_M = R \tag{19}$$

and recalculate T_1 to make this relation precisely true. Then we approximate a(r) by

$$a^{(m)}(r) = c_0^{(m)} + c_1^{(m)} r \qquad b_{m-1} \leq r \leq b_m \tag{20}$$

by equating a(r) to the numerically calculated values at the segment boundaries. This yields

$$\frac{1}{\alpha_i} = \frac{a(b_o)}{\rho_i} + \sum_{m=1}^{M-1} \frac{a(b_m) - a(b_{m-1})}{b_m - b_{m-1}} \left[\ln\ b_m - \ln\ b_{m-1}\right] \tag{21}$$

This algorithm yields good accuracy with less steps than were required by the previous one. One has two choices: (i) speed up the code greatly with systematic

errors in the integration similar to those in SM2 and SM3 or (ii) speed up the code slightly with greatly improved convergence of the integrations. We chose the latter option as the basis of our parameterization for SM2.1 and the various SM4-type models. The default values of T_1 and F for SM2.1 and SM4-type models are $T_1 = 0.15$ Å and F = 0.20, but in cases where speed is of the essence the user may opt for lower levels of convergence. The user may also run in fixed-M mode in cases where strict continuity of the results as a function of geometry or initial guess is important.

SCF Convergers As is well known, self-consistent fields governing the motions of electrons in molecular orbital calculations are achieved numerically by an iterative process. In gas-phase calculations the field in question is supplied by the nuclei and the other electrons. For molecules in solution, the free energy of solvation also contributes to the field, i.e., to the Fock operator *(25)*. In devising an iterative strategy (which is *always* more of an art than a science), we should keep in mind that an update of the solvation terms is more costly than several SCF cycles with frozen solvation terms, with the precise value of "several" increasing with the average value of M in Section 3. Therefore an efficient code will need to be able to freeze or unfreeze the updates to the solvation terms in the Fock operator by some adaptive procedure. One must balance costs, though, against the counterconvergent nature of making an update after several cycles with frozen solvent if that update is too abrupt. Versions 4.0 and later of AMSOL involve damped updates at adaptively selected cycles. If the SCF converges without problems, damping is rapidly decreased. If problems are encountered, then, at first the damping factor is increased. If this does not cure the bad convergence, a damped level shift option is employed as the method of last resort.

4. New Charge Model

The traditional approach to semiempirical molecular orbital theory has placed all the parameters in the Hamiltonian, or equivalently in the Fock operator. Then, having obtained a wave function, it is used and analyzed by the same methods as if it were an *ab initio* wave function (e.g., Mulliken analysis *(11-13)*, electrostatic potential fitting *(40-42)*, etc.). We have recently proposed a new class of charge models that use a different philosophy *(18)*. In particular an additional semiempirical layer is inserted between the semiempirical wave function and the physical observables inferred from it. This is accomplished by mapping partial charges obtained from the semiempirical wave function onto a new set of charges, q_k^{CM}, with the parameters of the mapping itself obtained from a general or specific parameterization. Like partial charge models based on fitting discrete charge representations to electrostatic potentials calculated from the full continuous wave electronic probability densities, the CM charge models make up for the errors inherent in using a discrete set of partial charges, but unlike electrostatic fitting charges, they also make up for the deficiencies *(42c)* of the electronic structure level and basis set employed because the parameters are fit to experimental data.

In the new charge models, the mapping occurs in two stages. The semiempirical Mulliken charge, $q_k^{(0)}$, for a given atom, k, is first adjusted by a parameterized change Δq_k,

$$q_k = q_k^{(0)} + B_k \Delta q_k, \tag{22}$$

In the second step of the mapping, the partial charges are readjusted to force the total charge on the molecule or ion to be the proper integral value (zero for neutrals). This is done by shifting charge locally between each atom whose charge has been adjusted and the atoms to which it has nonzero bond order. The final partial charge is then

$$q_k^{CM} = q_k^{(0)} + B_k \Delta q_k - \sum_{k' \neq k} B_{kk'} \Delta q_{k'} \tag{23}$$

where $B_{kk'}$ is the covalent bond index *(31)* between atoms k and k′. The sum of the bond orders from atom k to all other atoms is B_k. The following sum serves to ensure the charge is conserved in the mapping.

$$B_k = \sum_{k' \neq k} B_{kk'}. \tag{24}$$

where B_k is the sum of the covalent bond indices of atom k to all other atoms.

In work published elsewhere *(18)* we present new general parameterizations of such charge models, based on a large database of ions and neutrals. In the present study we use an early version parameterized only against neutral molecules. In the version we use here, $q_k^{(0)}$ is obtained by Mulliken analysis of the AM1 wave function, and Δq_k is obtained by

$$\Delta q_k = \begin{cases} -0.0283 & k = O \\ 0.1447 \sum_{k'} B_{kk'} & k = H,\ k' = O \\ 0 & k = C \end{cases}, \tag{25}$$

The parameters in eq. (25) were obtained from a database including 12 alcohols, 8 esters and lactones, 16 aldehydes and ketones, 9 acids, and 10 ethers. The root mean square (RMS) error between dipole moments derived from the new point charges and experimental dipole moments is 0.23 Debye for these 55 compounds. Point-charge dipole moments calculated from the unmodified AM1 Mulliken charges for the same set have an RMS error of 0.48 Debye. A comparison between dipole moments derived from the new point charges and those from the ab initio HF/6-31G* density or electrostatic potential for 7 representative members of the set (methanol, methyl formate, formaldehyde, cyclopropanone, acetic acid, dimethyl ether, and tetrahydrofuran) showed errors (compared to experiment) of 0.29 Debye for the dipoles from CM charges, 0.31 Debye for the dipoles from the Hartree-Fock density,

and 0.31 Debye again for the dipoles corresponding to charges obtained from Hartree-Fock electrostatic potential. The electrostatic fitting was carried out by the ChelpG method *(42a,b)*.

Of course, as for any semiempirical method, there is the possibility that unphysical results will be obtained for compounds dissimilar to the test set used in development, but since the algorithm is linear and the test set contains diverse elements, such problems are not expected to be serious. Figure 1 compares the partial atomic charges for one example, benzaldehyde, which was not in the data set used for parameterization, as calculated at a variety of levels. The excellent perform-

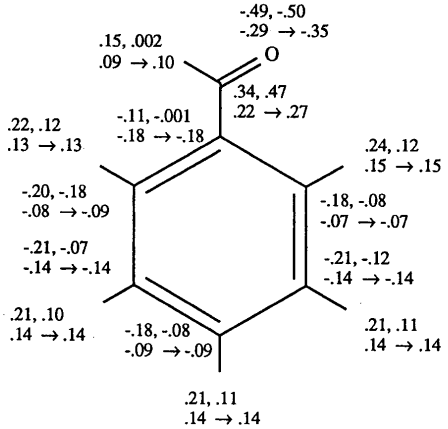

Experiment	μ = 2.8
Mulliken, ChelpG	4.0, 3.5
AM1 → AM1-CM	2.6 → 2.9

Figure 1. Partial charges and dipole moments (in Debye) for benzaldehyde. Next to each atom are shown four partial charges. Row 1 contains partial charges calculated by Mulliken analysis (given first) and ChelpG analysis of the HF/6-31G* wave function at the HF/6-31G* optimized geometry. Row 2 contains partial charges calculated by Mulliken analysis or the new charge model form the AM1 wave function at the AM1 optimized geometry. Below the molecule is given the experimental dipole moment, and below that are given dipole moments calculated from each of the four sets of partial charges described above in the same order.

ance of the new charge model for this molecule, as judged by its comparison to both the experimental dipole moment *(43)* and that derived from the MP2/6-31G* continuous density, illustrates the robust nature of the mapping. Of particular note is the effect of the mapping on the carbonyl bond dipole, which is considerably increased relative to the AM1 Mulliken charge result. The polarization is still larger for the HF/6-31G* Mulliken or electrostatic-potential fitted charges, but these methods both lead to charges that overestimate the dipole moment derived therefrom.

The utility of the more accurate charges yielded by the new charge model is discussed below in the context of solvation modeling.

We note that in SM1, SM1a, SM2, SM3, and SM2.1, the electrostatic term, ΔG_{ENP}, suffers deficiencies from the inaccuracy of the AM1 and PM3 charge distributions. These are absorbed into the parameterized surface tensions. Solvation models based on charges obtained from the new kind of charge model, on the other hand, are called SM4-type solvation models, e.g., SM4A, SM4C, SM4-SRP, and are expected to be less prone to such systematic deficiencies.

5. Specific Reaction Parameters for the Claisen Rearrangement

The critical step in the advancement of semiempirical molecular orbital theory from a promising approach studied by theoretical chemists to an everyday tool in the laboratory was the development of general parameterizations, such as CNDO/2 *(44)*, INDO/S *(45)*, MINDO/3 *(46)*, etc. The current working-horse general parameterizations are AM1 *(16)* and PM3 *(17)*. General parameterizations are not, however, the only way in which semiempirical molecular orbital theory can be useful. For example, one may want to study a particular class of compounds for which the general parameterization is known to have systematic errors. Alternatively, one may not have sufficient experimental data or enough time available to calibrate a general parameterization for a particular solvent at a given level of theory. In such cases, a parameterization for a specific range of compounds or an individual reaction might be useful. We call this an SRP model, as mentioned in the introduction. SRP-type models have been used for gas-phase studies of reaction dynamics *(47-49)*; we apply them here to solvation. The original goal of developing SRP models is to provide a convenient and flexible way of studying specific reactions or ranges of compounds, but another possible use would be to illuminate the *nature* of the deficiencies of general models.

In this section we present SRP solvation model in both water and hexadecane as an example of the new approach. The organic reaction in this case is the Claisen rearrangement, a [3,3] sigmatropic shift which converts an allyl vinyl ether into a γ,δ-unsaturated aldehyde (Figure 2). The reaction itself will be discussed more fully inthe next section. Here, we first select a data set, and then we select a functional form for the SRP parameterization. The SRP solvation model that is presented in this section will be denoted SM4-SRP where the 4 denotes that it is based on CM-type charges, as explained at the end of Section 4. More specifically, we use the AM1 Hamiltonian and CM charges so an unnecessarily complete but more descriptive name is AM1-CM-SM4-SRP, just as SM2 may be called AM1-SM2 to emphasize the Hamiltonian.

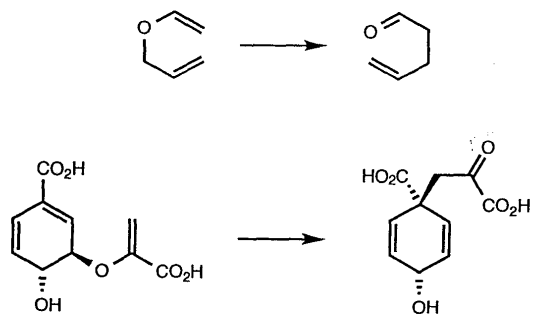

Figure 2. The Claisen rearrangement converts allyl vinyl ether to 4-pentenal. Also shown is the Claisen rearrangement which converts chorismic acid into prephenic acid, and important step in the biosynthetically important shikimic acid pathway.

An appropriate data set for determining SRP parameters for the Claisen rearrangement should include alkanes, alkenes, six-membered rings, ethers, aldehydes, and conjugated double bonds, since these are the functional groups involved in the reactants, products, and transition state. Within this range, we choose a representative set of molecules based on the availability *(34-37)* of experimental free energies of solvation. The number of parameters to be determined was reduced to a minimum by setting all $d_{ii}^{(1)} = 0$. Parameters $\sigma_i^{(1)}$ for the SM4-SRP model are defined to be zero. The optimal values of the SRP parameters are provided in Table 1, and the performance of the SRP models for the parameterization test set is detailed in Table 2. The hexadecane SRP model has an encouragingly small overall root-mean-square (RMS) error of 0.5 kcal/mol. The water SRP model is good at predicting the hydrophobic effect for hydrocarbons; it exhibits somewhat larger errors for the {C,H,O} compounds, with a tendency to underestimate the solvation free energies of ethers while overestimating those for aldehydes. Similar behavior was noted for SM2 *(5,7)*.

6. Solvation Effects on the Claisen Rearrangement

The Claisen rearrangement is an electrocyclic reaction converting an allyl vinyl ether into an unsaturated aldehyde or ketone via a [3,3] sigmatropic shift (Figure 2).

Table 1 . Optimized parameters for the Claisen SM4-SRP models (distances are in Ångstroms, charges in electronic charge units, and surface tensions in cal mol^{-1} Å^{-2})

	Water			*n*-Hexadecane		
Parameter	H	C	O	H	C	O
$\rho_k^{(0)}$	0.590	1.798	1.350	0.590	1.798	1.350
$\rho_k^{(1)}$	1.283	0.000	0.000	1.283	0.000	0.000
$q_k^{(0)}$	–0.300	0.000	0.000	–0.300	0.000	0.000
R_k	1.200	1.700	2.000	1.200	1.700	2.000
$\sigma_k^{(0)}(1)$	8.886	–6.910	–6.424	–48.000	–56.200	–42.900
$\sigma_k^{(0)}(2)$				16.700	16.700	16.700
$R_S(1)$	1.400	1.400	1.400	2.000	2.000	2.000
$R_S(2)$				4.900	4.900	4.900

Table 2. Calculated SM4-SRP and experimental free energies of solvation (kcal/mol) for hydrocarbons, aldehydes, and ethers

	Water				*n*-Hexadecane			
	Calculated				Calculated			
	ENP	CDS	Total	Expt.	ENP	CDS	Total	Expt.
Hydrocarbons								
ethane	–0.05	1.38	1.33	1.83	–0.03	–0.60	–0.63	–0.66
propane	–0.03	1.66	1.62	1.96	–0.02	–1.34	–1.36	–1.42
butane	0.01	1.93	1.94	2.08	0.01	–2.08	–2.07	–2.19
pentane	0.06	2.20	2.26	2.38	0.03	–2.82	–2.79	–2.94
2–methylpropane	0.00	1.82	1.82	2.32	0.00	–1.99	–1.99	–1.91
hexane	0.12	2.47	2.59	2.49	0.06	–3.55	–3.49	–3.63
2–methylpentane	0.10	2.28	2.38	2.88	0.05	–3.29	–3.24	–3.45
cyclohexane	0.04	2.25	2.30	1.23	0.02	–2.64	–2.62	–3.96
heptane	0.17	2.75	2.92	2.62	0.09	–4.29	–4.20	–4.32
2,4–dimethylpentane	0.16	2.41	2.57	2.88	0.08	–3.87	–3.79	–3.87
octane	0.23	3.02	3.25	2.89	0.12	–5.03	–4.91	–5.01
neopentane	0.02	1.94	1.97	2.50	0.01	–2.53	–2.52	–2.47
benzene	–2.12	0.88	–1.24	–0.87	–1.03	–2.71	–3.74	–3.81

Continued on next page

Table 2. Continued

	Water				*n*-Hexadecane			
	Calculated				Calculated			
	ENP	CDS	Total	Expt.	ENP	CDS	Total	Expt.
toluene	–2.11	1.23	–0.88	–0.89	–1.02	–3.35	–4.37	–4.55
o–xylene	–2.15	1.50	–0.65	–0.90	–1.01	–4.00	–5.01	–5.36
m–xylene	–2.10	1.58	–0.52	–0.84	–1.05	–3.87	–4.92	–5.26
p–xylene	–2.08	1.59	–0.49	–0.81	–1.00	–4.00	–5.00	–5.25
RMS error			**0.42**				**0.37**	
{H,C,O} cmpds								
dimethyl ether	–2.19	0.83	–1.36	–1.90	–1.62	–0.39	–2.01	–1.67
diethyl ether	–1.74	1.74	0.00	–1.63	–1.44	–1.15	–2.59	–2.47
dipropyl ether	–1.39	2.31	0.92	–1.15	–1.35	–1.88	–3.23	–3.09
diisopropyl ether	–1.36	2.10	0.74	–0.53	–1.41	–2.62	–4.03	–3.77
dibutyl ether	–1.25	2.85	1.60	–0.83	–2.11	–3.13	–5.24	–5.43
anisole	–3.55	0.84	–2.71	–2.44	–1.29	–3.36	–4.65	–4.59
tetrahydropyran	–1.96	1.56	–0.40	–3.12	–1.26	–4.10	–5.36	–5.26
dioxane	–3.59	0.85	–2.74	–5.05	–1.23	–4.83	–6.06	–5.96
phenetole	–3.32	1.31	–2.01	–2.21	–1.20	–5.57	–6.77	–6.68
acetaldehyde	–5.22	0.28	–4.94	–3.50	–0.74	–0.78	–1.52	–1.28
propanal	–4.57	0.70	–3.87	–3.44	–0.63	–2.49	–3.12	–2.80
butanal	–4.30	0.97	–3.33	–3.18	–0.49	–3.97	–4.46	–4.07
pentanal	–4.26	1.24	–3.02	–3.03	–0.50	–3.67	–4.17	–3.48
benzaldehyde	–5.79	0.19	–5.60	–4.02	–0.42	–5.44	–5.86	–5.45
hexanal	–4.17	1.52	–2.65	–2.81	–1.52	–3.45	–4.97	–5.35
heptanal	–4.13	1.79	–2.34	–2.67	–0.71	–2.18	–2.89	–4.07
octanal	–4.06	2.06	–2.00	–2.29	–1.35	–1.72	–3.07	–3.84
nonanal	–4.01	2.33	–1.68	–2.08	–1.42	–4.30	–5.72	–5.64
E–2–hexenal	–5.68	0.53	–5.15	–4.63				
E–2–butenal	–5.62	0.41	–5.21	–4.22				
E,E–2,4–hexadienal	–5.26	1.03	–4.23	–3.68				
E–2–octenal	–5.16	1.57	–3.59	–3.44				
RMS error			**1.25**				**0.59**	

The reaction has demonstrated synthetic utility *(50-52)*. The Claisen rearrangement has the additional distinction of being one of the few electrocyclic reactions which has been demonstrated to occur in a biosynthetic pathway; in particular, the rearrangement of chorismic acid to prephenic acid, catalyzed by the enzymatic influence of chorismate mutase, plays a role in the shikimic acid pathway of primary plant metabolism *(53-55)* This has prompted the development of antibodies capable of catalyzing the Claisen rearrangement *(56,57)*.

The Mechanism of the Claisen Rearrangement. Studies of the Claisen rearrangement have focused on several different mechanistic aspects of the reaction. One question of interest has been the degree of C–O bond breaking/C–C bond making which characterizes the transition state as inferred from analysis of kinetic isotope effects in the rearrangement *(58-63)*. Experimental results suggest that C–O bond breaking is significantly advanced over C–C bond making, leading to a transition state which involves two comparatively weakly coupled three-heavy-atom fragments *(58,59,62)*. Although early computational studies at the MNDO level were not in agreement with such an analysis *(60)*, more reliable levels of theory, including ab initio RHF calculations *(61)*, AM1 semiempirical calculations *(64)*, and MCSCF calculations *(63)*, all support the experimental interpretation.

An additional question of interest with respect to the Claisen transition state has been the extent to which it is characterized by interfragment charge separation and/or biradicaloid character. Figure 3 illustrates some of the limiting possibilities. Transition state **i** corresponds to the situation predicted by MNDO calculations *(60)*: C–C bond making is advanced over C–O bond breaking, and the overall character of the transition state is biradicaloid, that is, there are strong through-bond interactions

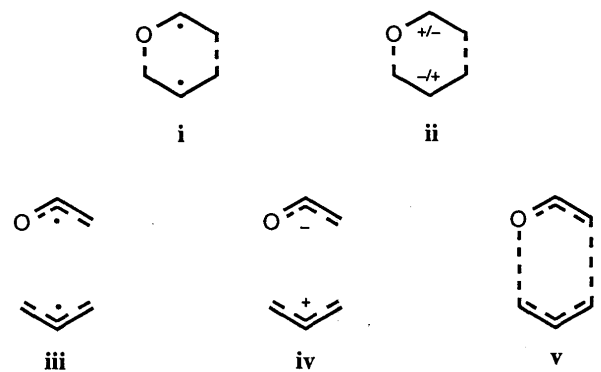

Figure 3. Limiting resonance structures which may be used to represent the transition state of the Claisen rearrangement.

between the oxallylic and allylic radical fragments. Alternatively, transition state **ii** corresponds to a similar situation with respect to relative bond making/breaking, but the fragments are more zwitterionic-like—although this structure is presented for completeness, it has never been suggested to be germane to the Claisen rearrangement.

Transition state **iii** corresponds to the case in which the interfragment coupling is considerably weaker (i.e., bond breaking is now advanced over bond making) with the character of the TS being close to a diradical (i.e., the net charges on the two fragments are near zero). The distinction between a transition state which is a "diradical" and one which has "biradicaloid" character is that there is no significant interaction between the radical centers in the former, but there is in the latter. Transition state **iv** resembles **iii**, except that the character of the TS is zwitterionic, being well described as a combination of an enolate anion and an allylic cation. Finally, transition state **v** refers to an "aromatic" transition state. This term was coined by Dewar to refer to a pericyclic transition state which (i) has roughly equal bond making and bond breaking and (ii) enjoys significant resonance stabilization from the mixing of the various molecular orbitals playing a significant role in the rearrangement even though the interfragment separation is large compared to the biradicaloid case **i** *(65)*. Since the aromatic MO's are delocalized, such a transition state may or may not be zwitterionic (and therefore synonymous with **iv**), but it is not a diradical.

Experimental studies have attempted to investigate the most likely character of the transition state by examination of substituent and solvent effects on the rate of the rearrangement. Based on rate accelerations observed in polar solvents, and sensitivity to substituent positioning, several groups have advocated the dipolar transition state **iv**/**v** *(66-70)*. However, Gajewski and co-workers have been reluctant to interpret the data similarly, and have suggested that a transition state **v** with quite limited dipolarity is more reasonable *(69,71)*.

Gas-phase modeling has been unable to provide a definitive answer since, at least for the parent allyl vinyl ether, the transition state structure proves extremely sensitive to the level of theory employed. At the RHF/6-31G* level of theory, the transition state has an interfragment distance (defined as the average of the breaking and forming C–O and C–C bonds, respectively) of about 2.1 Å. The enolate and allyl fragments have charges of –0.34 and 0.34 electrons, respectively, as analyzed from Mulliken population analysis *(61,63)*. Optimization at the MP2/6-31G* level gives a transition state structure which is slightly more biradicaloid in character, and kinetic isotope effects based on calculated harmonic frequencies are in poor agreement with experiment *(63)*. At the MCSCF level, on the other hand, correlating six electrons in six orbitals delivers a transition state structure which is much closer to transition state **iii**, with the distance between fragments increased to roughly 2.3 Å and the charge separation reduced to ±0.16 electrons on each fragment *(63)*. The "true" transition state structure in the gas phase may be a little tighter than the MCSCF one due to dynamical electron correlation.

Calculations at the semiempirical AM1 level, by contrast, led Dewar to suggest that both biradicaloid (**i**, interfragment separation about 1.7 Å) and aromatic (weakly dipolar **v**, interfragment separation about 1.8 Å) transition states exist,

corresponding to different reaction paths *(64,72)*. This analysis relies, however, on a somewhat dubious interpretation *(72)* of the molecular hypersurface. Although a similar bifurcation of reaction path was observed from MCSCF computational results obtained for the Cope rearrangement *(73,74)*, which is the all carbon analog of the Claisen (i.e., the oxygen atom is replaced by a methylene group), inclusion of dynamical correlation suggests there to be only a single reaction path *(75)*.

A conservative interpretation of all of these results taken together is that the nature of the Claisen rearrangement transition state is quite sensitive to external perturbations, whether those perturbations be in the form of structural modifications of the parent allyl vinyl ether fragments or in the form of differences in environmental conditions such as introducing or changing a solvent. With this caveat in mind, however, it remains interesting to consider what kinds of interactions with the surrounding solvent give rise to the phenomenologically observed rate accelerations of Claisen rearrangements in solvents of increasing polarity *(66,68-71)*. A number of computational studies employing quite different techniques have been undertaken with this goal in mind *(76-80)*, and we devote the remainder of this section to their comparison and critical analysis.

Modeling the Claisen Rearrangement in Solution. Two of the present authors performed the first computational study of the effect of solvent on the Claisen rearrangement, employing a GB/ST-type model, in particular SM2 *(76)*. In addition to the parent system, allyl vinyl ether, this study also considered all possible substitutions of a methoxy group for a proton in the molecule. Aqueous acceleration of the Claisen rearrangement was accounted for by electric polarization and first-hydration-shell hydrophilic effects. Polarization was found to dominate, although the relative magnitudes and even the signs of the two effects were quite sensitive to the substrate substitution pattern. Hydrophobic acceleration, from the joining together of the two terminal methylene groups in the transition state, was found to be accelerating as well, but only worth about 0.3 kcal/mol in every case. The SM2 calculations indicated that solvent polarization in the parent and methoxy-substituted systems tended to be most responsive to the oxygen atoms because of their smaller volume and moderately large charges. Geometrical changes on going from the reactant conformation to the transition state which sequestered charges of opposite sign into well separated regions of space contributed to rate acceleration, while the converse was true when charges of opposite sign were forced into proximity. Although the *intra*fragment charges were consistent with the enolate/allyl cation view of the transition state, i.e., negative charge buildup at either end of the former fragment and positive charge buildup at either end of the latter, the *inter*fragment charge separation was fairly small at only 0.14 electrons from Mulliken population analysis (Table 1). While this charge reorganization was related to the increase or decrease in overall dipole moment on progressing to the transition state, consideration of only the dipole moment proved insufficient to reproduce the distributed-monopole results of the SM2 model. Because competing axial and equatorial substitution patterns and competing chair and boat transition states involved different spatial arrangements of the critical charges, it was shown that energetic discrimination between competing reaction

routes delivering stereochemically different products could be substantially changed in water in comparison to the gas phase or to nonpolar solvents.

The SM2 calculations led to a rate acceleration of 3.5 on going from the gas phase to aqueous solution at 298 K. Such quantitative predictions form the SM2 model are less reliable than the qualitative insights for two reasons: first, biradicals (and often zwitterions) require configuration interaction (CI) for an accurate representation of the electronic wave function, and the AM1 electronic structure level employed in the SM2 calculations does not allow for this; second, the AM1 Mulliken charges used in SM2 are not quantitatively accurate.

Severance and Jorgensen *(77)* analyzed the available experimental results and suggested that a more accurate rate acceleration would be on the order of 1000 at 348 K. These authors calculated the gas-phase reaction coordinate at the HF/6-31G* level for the Claisen rearrangement, and then solvated structures chosen periodically along that gas-phase path using Monte-Carlo simulations *(81)* employing the 4-Point Transferable Intermolecular Potentials (TIP4P) water model *(82)*, Optimized Potentials for Liquid Simulations (OPLS) van der Waals parameters *(83)*, and electrostatic-potential-derived HF/6-31G* atomic partial charges in order to generate an aqueous reaction coordinate. The simulations suggested a rate acceleration of 644 at 298 K, in good agreement with the extrapolated factor of about 1000. Analysis of the simulations revealed enhanced hydrogen bonding to oxygen in the transition state (1.9 average total number of hydrogen bonds) by comparison to the starting ether (0.9 average). This enhanced hydrogen bonding arises in part from increased accessibility of the oxygen atom in the transition state and also from its increased charge; in the gas-phase calculations from which the partial charges were taken, the oxygen becomes more negative by 0.07 electrons *(80)*.

The AM1-SM2 quantum mechanical continuum model and the HF/6-31G*-OPLS-TIP4P explicit water simulation agreed nicely on one point of particular interest. As noted in a short commentary that summarized them *(84)*, "Both studies show that reorganization of the charge distribution is more subtle and not in accord with an ion pair-like transition state. Rather polarization occurs within the enolate moiety of the transition state, rendering the oxygen more negative." Moreover, both studies indicated the bulk of the acceleration to be associated with improved solvation of the oxygen atom portion of the molecule.

Gao recently reported a study of the Claisen rearrangement which complements the earlier two in an extremely interesting way *(78)*. Taking the same gas-phase reaction coordinate as Severance and Jorgensen, Gao performed combined QM/MM *(85)* simulations in which the solute was modeled using the AM1 Hamiltonian and OPLS van der Waals parameters, with the quantum mechanical Hamiltonian perturbed by surrounding explicit water molecules treated classically using the TIP3P *(82)* water model. This approach thus includes electronic polarization of the solute, together with explicit simulation of the solvent. The rate acceleration (gas phase → aqueous solution) calculated by Gao was 368 at 298 K. Gao emphasized several points of agreement between his study and those of the earlier authors. As before, charge buildup at oxygen was identified as the primary contributor to rate acceleration. In addition, little interfragment charge separation was observed in either the gas-phase or the solution electronic structures. Moreover, solute polarization in the transition state was calculated by Gao to account for 35% of the rate acceleration, in good agreement with the SM2 results. Although the study of Severance and Jorgensen does not explicitly account for solute polarization, charges derived from HF/6-31G* calculations appear to be systematically too large, and thus to some extent they mimic intrinsic incorporation of polarization effects.

Specific Reaction Parameter Modeling of the Claisen Rearrangement in Solution. The sensitivity of the rate acceleration to atomic partial charges and as well the sensitivity of the transition state structure to level of theory prompted us to investigate more closely the dependence of calculated rate acceleration on these factors within the SMx series of models. We have therefore calculated the rate accelerations for the aqueous Claisen rearrangement using both the SM2 and SM4-SRP models, in each case employing three choices of transition state geometry: (i) self-consistently optimized (in solution) chair transition states, (ii) the HF/6-31G* gas-phase transition state, and (iii) the MCSCF/6-31G* gas-phase transition state. The partial charges calculated for these different possibilities are presented in Table 3, and the accelerations are listed in Table 4. Several points warrant further discussion.

(i) First, it is obvious that looser transition states give rise to greater acceleration. This acceleration derives partly from larger atomic partial charges, with effects at oxygen predominating, and partly from greater accessibility of hydrophilic sites to solvent. It is especially interesting to note the synergistic effect of using both better transition state structures and a better charge model: the accelerations calculated by SM2 and SM4-SRP models are essentially identical at the semiempirically optimized transition state structure, which has the reacting fragments too tightly coupled. As the transition state structure becomes looser, the SM4-SRP model predicts steadily enhanced acceleration over the SM2 model, although the latter model itself predicts roughly 80-fold acceleration on going from the semiempirically optimized TS structure to the MCSCF gas-phase TS structure. Since the true transition state structure is probably looser than the HF/6-31G* one, and the looser transition state gives rise to larger aqueous acceleration, calculations based on the HF/6-31G* wavefunction and gas-phase reaction path should not give the quantitatively correct acceleration.

(ii) For the tight semiempirical case, it is interesting to note that bringing the methylene termini closer together in the transition state structure gives rise to a hydrophobic acceleration in water; however, this same change in structure corresponds to a solvo*phili*c *de*celeration in hexadecane. In the latter case, the effect is sufficient to slow the reaction down relative to the gas phase! As expected, this effect becomes smaller in magnitude for both solvents in the looser transition states, in particular by 0.1 kcal/mol for water and 0.2 kcal/mol for hexadecane.

(iii) If the polarization free energies were to be calculated using the gas-phase partial charges, it is clear that water as solvent would give about twice the polarization as hexadecane—this follows from the difference in the dielectric constants of the two solvents and how that difference modifies the pre-factor on the right-hand side of eq. 3. This analysis suggests, using simple transition state theory and temporarily ignoring the small differences in $\Delta G^{o,\ddagger}_{CDS}$, that the rate acceleration in water

Table 3. Partial charges (including attached hydrogens) in Claisen chair transition state

TS geometry	C-1	C-2	O-3	C-4	C-5	C-6	Charge separation[a]
Mulliken gas-phase charges[b]							
AM1	0.01	0.10	–0.25	0.20	–0.17	0.10	0.14
HF/6-31G*[c]	–0.14	0.41	–0.61	0.34	0.00	0.00	0.34
MCSCF/6-31G*[d]	–0.04	0.35	–0.47	0.10	0.06	0.01	0.16
CM gas-phase charges							
AM1	0.01	0.14	–0.30	0.22	–0.17	0.10	0.15
HF/6-31G*	–0.06	0.18	–0.38	0.23	–0.11	0.13	0.26
MCSCF/6-31G*	–0.09	0.18	–0.41	0.25	–0.09	0.14	0.32
SM2 water charges[e]							
SM2	0.03	0.10	–0.28	0.21	–0.18	0.13	0.15
HF/6-31G*	–0.06	0.14	–0.37	0.25	–0.12	0.17	0.29
MCSCF/6-31G*	–0.12	0.14	–0.43	0.30	–0.10	0.22	0.41
SM4-SRP water charges[e]							
SM4-SRP	0.04	0.13	–0.36	0.22	–0.18	0.13	0.19
HF/6-31G*	–0.06	0.18	–0.45	0.26	–0.12	0.19	0.33
MCSCF/6-31G*	–0.12	0.18	–0.52	0.32	–0.11	0.24	0.46
SM4-SRP hexadecane charges[e]							
SM4-SRP	0.02	0.10	–0.27	0.21	–0.17	0.11	0.15
HF/6-31G*	–0.06	0.14	–0.35	0.24	–0.11	0.15	0.27
MCSCF/6-31G*	–0.10	0.14	–0.40	0.27	–0.10	0.18	0.36

[a] Absolute value of total charge on the enolate/allyl fragments. [b] All geometries fully optimized, all charges at the same level of theory. [c] Reference *(61)*. Note that this report *(61)* typographically interchanged the charges for the chair TS and the starting ether, as made clear in reference *(63)*. Those errors were included in Table III of reference *(76)*. [d] Reference *(63)*. [e] SM*x* geometry optimized in solution, all others are frozen gas-phase structures.

Table 4. Solvent-induced rate acceleration of the Claisen rearrangement at 298 K

Solvation Model	Solvent	TS geometry	Rate Acceleration[a]
SM2	water	SM2	3.5[b]
		HF/6-31G*[c]	21
		MCSCF/6-31G*[d]	270
SM4-SRP	water	SM4-SRP	3.4
		HF/6-31G*	46
		MCSCF/6-31G*	1400
SM4-SRP	*n*-hexadecane	SM4-SRP	0.7
		HF/6-31G*	2.3
		MCSCF/6-31G*	11

[a] Gas phase to solution. [b] Reference *(76)*. [c] Gas-phase geometry from reference *(61)*. [d] Gas-phase geometry from reference *(63)*.

should be roughly the square of that in hexadecane. However, self-consistent *additional* polarization of the electronic structure by the solvent reaction field is *also* more favorable in water, and this effect accounts for roughly 10-fold more aqueous acceleration than would otherwise be expected. Such a prediction cannot be made using classical models with fixed atomic charges. The net result from the SRP models is a ratio of 124:1 for the rate of the Claisen rearrangement of allyl vinyl ether in water as compared to hexadecane. This is in excellent agreement with an experimentally observed ratio of 214:1 for the rates of related sets of Claisen rearrangements measured in water and cyclohexane *(71)*.

(iv) The self-consistent-field SM4-SRP charge separation between fragments is found to be 0.46 electrons at the MCSCF transition state structure. This value is somewhat larger than the 0.34 electron separation derived from electrostatic potential fitting of HF/6-31G* charges as used by Severance and Jorgensen in their Monte Carlo simulations. All of the computational studies, then, point to a moderate degree of interfragment charge separation; however, it is the *intra*fragment charge organization which is critical to the calculated rate accelerations.

(v) Finally, it is worth emphasizing that the above results are extremely useful in terms of understanding the mechanism of the Claisen rearrangement in the condensed phase, but are probably no better than semiquantitative in terms of predicting absolute rate accelerations. It is clear that accounting for dynamical correlation *and* for the effect of solvent on the reaction coordinate itself may significantly alter the structure of the transition state. Of course, these two effects

should be in opposite directions, dynamical correlation favoring a tighter structure and solvation a looser one, so there might be a fortuitous cancellation of errors in this instance.

In closing this section, it is appropriate to compare these results to the quite different approach used by Gajewski *(79)*, who has employed factor analysis to correlate the rate acceleration of the Claisen rearrangement in a wide variety of solvents against a series of empirical solvent descriptors. Gajewski suggests that solvent hydrogen bond donating ability is the factor most closely correlated with rate acceleration. This analysis clearly agrees with the Monte Carlo simulations of Severance and Jorgensen and of Gao, where enhanced hydrogen bonding is explicitly observed for transition state structures relative to reactants. Although the continuum model results presented here obviously do not include an explicit representation of the solvent, they are quite consistent with all of the other studies. In particular, the enhanced hydrogen bonding observed in the simulations is due primarily to the increased charge and increased accessibility of the oxygen atom in the Claisen transition state structure, and the continuum model finds rate acceleration to be similarly dependent on these two factors. Of course, it is not at all trivial to separate hydrogen bonding into electrostatic and non-electrostatic components, nor is it easy to separate electrostatic effects into hydrogen bonding and non-hydrogen-bonding components, and the extent to which those portions of experimental free energies of solvation assignable to hydrogen bonding effects are incorporated into the ENP and CDS terms of the SM*x* models is not clear. Thus, although the SM*x* results cannot be interpreted quantitatively in terms of hydrogen-bonding effects, they are not inconsistent with such effects dominating.

7. Summary and Concluding Remarks

We have presented an overview of recent improvements and extensions of the quantum mechanical generalized-Born-plus-surface-tensions SM*x* solvation models, and we illustrated a new way to treat reaction-specific solvation effects using the Claisen rearrangement as an example. General improvements discussed included more efficient algorithms in the AMSOL computer code for calculating analytical solvent accessible surface areas, for evaluating quadratures related to dielectric screening, and for solving the solvent-modified SCF equations. In addition, we have illustrated the use of class IV charge models. All of these improvements were used to develop a set of specific reaction parameters for calculating the effect of solvation on the Claisen rearrangement both in hydrocarbon solvent and in water. Calculated rate accelerations were in excellent agreement with the best available experimental estimates and also with other modeling approaches.

Acknowledgments. The authors are grateful to Ken Houk for providing a preprint of reference *(63)*. This work was supported in part by the National Science Foundation.

Literature Cited

(1) Daudel, R. *Quantum Theory of Chemical Reactivity*; Reidel: Dordrecht, 1973.
(2) Reichardt, C. *Solvents and Solvent Effects in Organic Chemistry*; VCH: New York, 1990.
(3) Kreevoy, M. M.; Truhlar, D. G. In *Investigation of Rates and Mechanisms of Reactions, Part I*; 4th ed.; C. F. Bernasconi, Ed.; Wiley: New York, 1986; p. 13.
(4) Cramer, C. J.; Truhlar, D. G. *J. Am. Chem. Soc.* **1991**, *113*, 8305.
(5) Cramer, C. J.; Truhlar, D. G. *Science* **1992**, *256*, 213.
(6) Cramer, C. J.; Truhlar, D. G. *J. Comp. Chem.* **1992**, *13*, 1089.
(7) Cramer, C. J.; Truhlar, D. G. *J. Comput.-Aid. Mol. Des.* **1992**, *6*, 629.
(8) Liotard, D. A.; Hawkins, G. D.; Lynch, G. C.; Cramer, C. J.; Truhlar, D. G. to be published.
(9) Storer, J. W.; Giesen, D. J.; Cramer, C. J.; Truhlar, D. G. to be published.
(10) Giesen, D. J.; Storer, J. W.; Cramer, C. J.; Truhlar, D. G. to be published.
(11) Mulliken, R. S. *J. Chem. Phys.* **1935**, *3*, 564.
(12) Mulliken, R. S. *J. Chem. Phys.* **1955**, *23*, 1833.
(13) Mulliken, R. S. *J. Chem. Phys.* **1962**, *36*, 3428.
(14) Pople, J. A.; Segal, G. A. *J. Chem. Phys.* **1965**, *43*, S129.
(15) Dewar, M. J. S.; Thiel, W. *J. Am. Chem. Soc.* **1977**, *99*, 4899.
(16) Dewar, M. J. S.; Zoebisch, E. G.; Healy, E. F.; Stewart, J. J. P. *J. Am. Chem. Soc.* **1985**, *107*, 3902.
(17) Stewart, J. J. P. *J. Comp. Chem.* **1989**, *10*, 209.
(18) Storer, J. W.; Giesen, D. J.; Cramer, C. J.; Truhlar, D. G. *J. Comp. Chem.* submitted for publication.
(19) Cramer, C. J.; Truhlar, D. G. In *Reviews in Computational Chemistry*; K. B. Lipkowitz and D. B. Boyd, Eds.; VCH: New York; Vol. 6; in press.
(20) Cramer, C. J.; Truhlar, D. G. In *Theoretical and Computational Chemistry: Solute/Solvent Interactions*; P. Politzer and J. S. Murray, Eds.; Elsevier: Amsterdam; Vol. 2; in press.
(21) Cramer, C. J.; Lynch, G. C.; Hawkins, G. D.; Truhlar, D. G. *QCPE Bull.* **1993**, *13*, 78.
(22) Hoijtink, G. J.; de Boer, E.; Van der Meij, P. H.; Weijland, W. P. *Recl. Trav. Chim. Pays-Bas* **1956**, *75*, 487.
(23) Peradejordi, F. *Cahiers Phys.* **1963**, *17*, 343.
(24) Jano, I. *Compt. Rend. Acad. Sci. Paris* **1965**, *261*, 103.
(25) Tapia, O. In *Quantum Theory of Chemical Reactions*; R. Daudel, A. Pullman, L. Salem and A. Viellard, Eds.; Reidel: Dordrecht, 1980; Vol. 2; p. 25.
(26) Born, M. Z. *Physik* **1920**, *1*, 45.
(27) Still, W. C.; Tempczyk, A.; Hawley, R. C.; Hendrickson, T. *J. Am. Chem. Soc.* **1990**, *112*, 6127.
(28) Hermann, R. B. *J. Phys. Chem.* **1972**, *76*, 2754.
(29) Hermann, R. B. *J. Phys. Chem.* **1975**, *79*, 163.
(30) Hermann, R. B. *Proc. Natl. Acad. Sci., USA* **1977**, *74*, 4144.
(31) Armstrong, D. R.; Perkins, P. G.; Stewart, J. J. P. *J. Chem. Soc., Dalton Trans.* **1973**, 838.
(32) Lazaridis, T.; Paulaitis, M. E. *J. Phys. Chem.* **1994**, *98*, 635.
(33) Alary, F.; Durup, J.; Sanenjouand, Y.-H. *J. Phys. Chem.* **1993**, *97*, 13864.
(34) Hine, J.; Mookerjee, P. K. *J. Org. Chem.* **1975**, *40*, 287.

(35) Cabani, S.; Gianni, P.; Mollica, V.; Lepori, L. *J. Solution Chem.* **1981**, *10*, 563.
(36) Abraham, M. H.; Whiting, G. S.; Fuchs, R.; Chambers, E. J. *J. Chem. Soc., Perkin Trans. 2* **1990**, 291.
(37) Zhang, Y.; Dallas, A. J.; Carr, P. W. *J. Chrom.* **1993**, *638*, 43.
(38) Pascual-Ahuir, J. L.; Silla, E. *J. Comp. Chem.* **1990**, *11*, 1047.
(39) Silla, E.; Tubon, I.; Pascual-Ahuir, J. L. *J. Comp. Chem.* **1991**, *12*, 1077.
(40) Rauhut, G.; Clark, T. *J. Comp. Chem.* **1993**, *14*, 503.
(41) Alhambra, C.; Luque, F. J.; Orozco, M. *J. Comp. Chem.* **1994**, *15*, 12.
(42) (a) Chirlian, L. E.; Francl, M. M. *J. Comp. Chem.* **1987**, *8*, 894. (b) Breneman, C. M.; Wiberg, K. B. *J. Comp. Chem.* **1990**, *11*, 361. (c) Merz, K. M. *J. Comp. Chem.* **1992**, *13*, 749.
(43) Liptag, W. In *Excited States*; E. C. Lim, Ed.; Academic Press: 1974; Vol. 1; p. 196.
(44) Pople, J. A.; Segal, G. A. *J. Chem. Phys.* **1966**, *44*, 3289.
(45) Ridley, J. E.; Zerner, M. C. *Theor. Chim. Acta* **1973**, *32*, 111.
(46) Bingham, R. C.; Dewar, M. J. S.; Lo, D. H. *J. Am. Chem. Soc.* **1975**, *97*, 1294.
(47) Gonzales-Lafont, A.; Truong, T. N.; Truhlar, D. G. *J. Phys. Chem.* **1991**, *95*, 4618.
(48) Viggiano, A. A.; Paschkewitz, J.; Morris, R. A.; Paulson, J. F.; Gonzales-Lafont, A.; Truhlar, D. G. *J. Am. Chem. Soc.* **1991**, *113*, 9404.
(49) Liu, Y.-P.; Lu, D.-H.; Gonzalez-Lafont, A.; Truhlar, D. G.; Garrett, B. C. *J. Am. Chem. Soc.* **1993**, *115*, 7806.
(50) Claisen, L. *Chem. Ber.* **1912**, *45*, 3157.
(51) Rhoads, S. J.; Raulins, N. R. *Org. React.* **1975**, *22*, 1.
(52) Ziegler, F. E. *Chem. Rev.* **1988**, *88*, 1423.
(53) Haslam, E. *The Shikimate Pathway*; Wiley: New York, 1974.
(54) Ganem, B. *Tetrahedron* **1978**, *34*, 3353.
(55) Bartlett, P. A.; Johnson, C. R. *J. Am. Chem. Soc.* **1985**, *107*, 7792.
(56) Hilvert, D.; Carpenter, S. H.; Nared, K. D.; Auditor, M.-T. M. *Proc. Natl. Acad. Sci., USA* **1988**, *85*, 4953.
(57) Jackson, D. Y.; Jacobs, J. W.; Sugasawara, R.; Reich, S. H.; Bartlett, P. A.; Schultz, P. G. *J. Am. Chem. Soc.* **1988**, *110*, 4841.
(58) Gajewski, J. J.; Conrad, N. D. *J. Am. Chem. Soc.* **1979**, *101*, 6693.
(59) McMichael, K. D.; Korver, J. L. *J. Am. Chem. Soc.* **1979**, *101*, 2746.
(60) Dewar, M. J. S.; Healy, E. F. *J. Am. Chem. Soc.* **1984**, *106*, 7127.
(61) Vance, R. L.; Rondan, N. G.; Houk, K. N.; Jensen, F.; Borden, W. T.; Komornicki, A.; Wimmer, E. *J. Am. Chem. Soc.* **1988**, *110*, 2314.
(62) Kupczyk-Subotkowska, L.; Saunders, W. H.; Shine, H. J.; Subotkowski, W. *J. Am. Chem. Soc.* **1993**, *115*, 5957.
(63) Yoo, H. Y.; Houk, K. N. *J. Am. Chem. Soc.* submitted for publication.
(64) Dewar, M. J. S.; Jie, C. *J. Am. Chem. Soc.* **1989**, *111*, 511.
(65) Dewar, M. J. S.; Ford, G. P.; McKee, M. L.; Rzepa, H. S.; Wade, L. E. *J. Am. Chem. Soc.* **1977**, *99*, 5069.
(66) Burrows, C. J.; Carpenter, B. K. *J. Am. Chem. Soc.* **1981**, *103*, 6983.
(67) Burrows, C. J.; Carpenter, B. K. *J. Am. Chem. Soc.* **1981**, *103*, 6984.
(68) Coates, R. M.; Rogers, B. D.; Hobbs, S. J.; Peck, D. R.; Curran, D. P. *J. Am. Chem. Soc.* **1987**, *109*, 1160.

(69) Gajewski, J. J.; Jurayj, J.; Kimbrough, D. R.; Gande, M. E.; Ganem, B.; Carpenter, B. K. *J. Am. Chem. Soc.* **1987**, *109*, 1170.
(70) Grieco, P. A. *Aldrichim. Acta* **1991**, *24*, 59.
(71) Brandes, E.; Grieco, P. A.; Gajewski, J. J. *J. Org. Chem.* **1989**, *54*, 515.
(72) Dewar, M. J. S.; Jie, C. *Acc. Chem. Res.* **1992**, *25*, 537.
(73) Dupuis, M.; Murray, C.; Davidson, E. R. *J. Am. Chem. Soc.* **1991**, *113*, 9756.
(74) Houk, K. N.; Gustafson, S. M.; Black, K. A. *J. Am. Chem. Soc.* **1992**, *114*, 8565.
(75) (a) Borden, W. T. In *Abstracts of the 207th National Meeting of the American Chemical Society*; American Chemical Society: Washington, DC, 1994; ORGN 129. (b) Hrovat, D. A.; Morokuma, K.; Borden, W. T. *J. Am. Chem. Soc.* **1994**, *116*, 1072.
(76) Cramer, C. J.; Truhlar, D. G. *J. Am. Chem. Soc.* **1992**, *114*, 8794.
(77) Severance, D. L.; Jorgensen, W. L. *J. Am. Chem. Soc.* **1992**, *114*, 10966.
(78) Gao, J. *J. Am. Chem. Soc.* **1994**, *116*, 1563.
(79) Gajewski, J. J.; Brichford, N. L. found elsewhere in this volume.
(80) Severance, D. L.; Jorgensen, W. L. found elsewhere in this volume.
(81) Jorgensen, W. L. *Acc. Chem. Res.* **1989**, *22*, 184.
(82) Jorgensen, W. L.; Chandrasekhar, J.; Madura, J. D.; Impey, R. W.; Klein, M. L. *J. Chem. Phys.* **1983**, *79*, 926.
(83) Jorgensen, W. L.; Tirado-Rives, J. *J. Am. Chem. Soc.* **1988**, *110*, 1657.
(84) Houk, K. N.; Zipse, H. *Chemtracts — Org. Chem.* **1993**, *6*, 51.
(85) Gao, J. *J. Phys. Chem.* **1992**, *96*, 537.

RECEIVED May 24, 1994

"Solvation Modeling in Aqueous and Nonaqueous Solvents: New Techniques and a Re-examination of the Claisen Rearrangement," J. W. Storer, D. J. Giesen, G. D. Hawkins, G. C. Lynch, C. J. Cramer, D. G. Truhlar, and D. A. Liotard, in *Structure, Energetics, and Reactivity in Aqueous Solution: Characterization of Chemical and Biological Systems*, edited by C. J. Cramer and D. G. Truhlar (American Chemical Society Symposium Series 568, Washington, DC, 1994), pp. 24–49.